Nanoscale

Accepted Manuscript

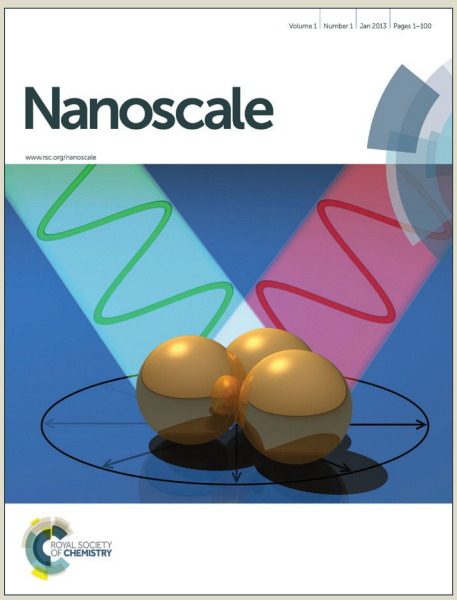

ROYAL SOCIETY OF CHEMISTRY

www.rsc.org/nanoscale

Inkjet-printed all solid-state electrochromic devices based on NiO/WO_3 nanoparticles complementary electrodes

Guofa Cai[a], Peter Darmawan[a], Mengqi Cui[a], Jingwei Chen[a], Xu Wang[a], Alice Lee-Sie Eh[a], Shlomo Magdassi[b], Pooi See Lee[a,*]

Author Address: [a]*School of Materials Science and Engineering, Nanyang Technological University, 639798, Singapore*

[b]*Institute of Chemistry and the Center for Nanoscience and Nanotechnology, The Hebrew University of Jerusalem, Jerusalem, 91904, Israel*

[*]Corresponding Author

E-mail: pslee@ntu.edu.sg

Abstract

Nanostructured and thin films are important in the fields of energy conversion and storage. Especially, multi-layered nanostructured films will play an important role as a part of the energy system for the energy saving applications in buildings. Inkjet printing is a low-cost and attractive technology for patterning and deposition of multi-layered nanostructured materials on various substrates. However, it requires the development of a suitable ink formulation with optimum viscosity, surface tension and evaporation rate for various materials. In this study, a versatile ink formulation was successfully developed to prepare NiO and WO_3 nanostructured films with strong adhesion to ITO coated glass using inkjet printing for energy saving electrochromic applications. We achieved a high performance electrochromic electrode, producing porous and continuous electrochromic films without aggregation. NiO film with 9 printed layers exhibits an optical modulation of 64.2% at 550 nm and coloration efficiency (CE) of 136.7 cm^2 C^{-1}. An inkjet-printed complementary all solid-state device was assembled, delivering a larger optical modulation of 75.4% at 633 nm and higher CE of 131.9 cm^2 C^{-1} among the all solid-state devices. The enhanced contrast is due to the printed NiO film that not only performs as ion storage layer, but also as complementary electrochromic layer.

1. Introduction

With the increasing energy demand, there has been growing interests in search for methods to reduce energy consumption.[1-6] Electrochromism as a promising energy-saving and energy-conversion technology which can reversibly and persistently change their optical properties to intelligently control the amount of solar heat in response to changes in ambient temperature by electrochemical oxidation and reduction of the electrochromic materials.[7-9] Electrochromic device is a multilayer structure consisting of transparent conductor, electrochromic film, ion conductor and ion storage film. These devices attract considerable interest because of their potential applications, such as smart windows for energy efficient building, information displays, self-dimming rear mirrors for automobiles, electronic papers and switchable mirrors.[10-13] Large optical modulation, good optical memory and chemical stability are required for a high-performance electrochromic device. Nickel oxide (NiO) is known as one of the most popular anodic electrochromic materials and tungsten trioxide (WO_3) as one of the widely accepted cathodic electrochromic materials, both of which have been intensively investigated.[14-16] NiO and WO_3 are complementary electrode materials when they are integrated into one electrochromic device using lithium based electrolytes. They can be simultaneously colored and bleached with opposite polarity, therefore, increasing the optical modulation of the complementary device.

The usual methods for producing electrochromic nanostructured NiO and WO_3 films include sputtering[17,18], electrodeposition[19,20] and hydrothermal processing[21, 22]. Unfortunately, these methods do not meet the requirements of low cost and versatile processing for consumable electronic systems. Furthermore, additional requirements are imposed on the emerging electronics development, such as the need of patterning and multi-layered structures. In the past,

creation of specific patterns usually involves a subtractive approach such as expensive lithography process or additional masking steps, which results in the wasting of materials or high cost during the fabrication process. Inkjet printing is a low-cost and attractive additive manufacturing technology for patterning electrochromic materials on various substrates and allows deposition of electrochromic materials on a specific location with simultaneous thickness control by the number of printed layers. In addition, the inkjet printing can further integrate with roll-to-roll technology for industrial scale production. [23, 24] However, inkjet printing requires the development of versatile ink formulation with optimum viscosity, surface tension and evaporation rate to avoid formation of inhomogeneous film, irregular and deformed printed lines, cracks and so on. Despite the prior effort of inkjet patterning of NiO on thermistor[25] and multilayer ceramic[26], demonstration of inkjet printed NiO for electrochromics has not been realized before. With our earlier established work on inkjet patterning of WO_3 for electrochromic application,[27] we extend our efforts on the understanding of the effects of inkjet printing parameters such as number of printed layers and the annealing temperature on the electrochromic performance. In addition, although a few papers about inkjet-printed electrochromic devices were published recently, the devices were assembled by the same electrochromic materials on single or both electrodes and the optical modulation is still unsatisfactory.[28-31] Herein, we report the first inkjet-printed complementary all solid-state electrochromic device with one of the best performance till date, to the best of our knowledge.

We introduce a versatile ink formulation and prepare electrochromic NiO and WO_3 films by inkjet printing technique. The ink formulation can work well for both NiO and WO_3 nanoparticles. The electrochromic performances of the NiO films with increasing printed layers and various thermal treatment temperatures are investigated in detail. Subsequently, an all solid

electrochromic device was assembled with NiO film as ion storage layer, WO_3 film as electrochromic layer and poly(methyl methacrylate) (PMMA)-based polymer electrolyte as the solid electrolytes. Solid-state electrochromic device can avoid electrolyte leakage problem, allow the ease of handling, reduce the cost of device packaging and attain greater reliability. In order to keep consistent with already existed electrochromic window in some energy efficient building, the commercial indium tin oxide (ITO)-coated glass was used as the conductive transparent substrate. The resultant electrochromic device with inkjet printed NiO film as ion storage layer exhibits large optical modulation and high coloration efficiency.

2. Experimental section

Tert-butanol (anhydrous, ≥99.5%), nickel acetylacetonate (95% purity), metallic tungsten, hydrogen peroxide (30%), PMMA (M_w=996 000), propylene carbonate (PC, ≥99.7%), lithium perchlorate ($LiClO_4$, ≥95.0%), ethylene glycol (EG, ≥99.5%), acetonitrile (ACN, ≥99.8%) and diethylene glycol n-butyl ether (DB, ≥99%) were purchased from Sigma-Aldrich. All the chemicals were used without further purification.

2.1 Ink formulation:

The NiO nanoparticles were prepared according to the method of our previous work.[32] In brief 0.39 g nickel acetylacetonate was added into 42 ml tert-butanol under stirring, forming a light green suspension. Thereafter, the obtained solution was transferred into a Teflon lined stainless autoclave, and then the autoclave was sealed and heated at 200 °C for 24 h. Afterwards, the autoclave was cooled to room temperature under air cooling. Finally, the NiO precipitates in the solution were collected and dried in an oven at 60 °C. The WO_3 nanoparticles were synthesized based on a modified sol–gel route according to Costa et al.,[29] and as reported in our

previous work[27]. The NiO ink follows the similar formulation as the WO_3 ink, with DB, EG and DI water as the solvents (NiO: EG: DB: DI water=1: 2: 47: 50). The optimized concentration of the NiO is 1 wt.% in the ink (beyond this concentration there will be sedimentation after a few days). The surface tension and the viscosity of the NiO ink is 22.51 Nm/m and 6.59 cP, respectively. Both inks were stable under ambient conditions for several weeks without particle sedimentation and aggregation, and displayed good printability.

2.2 Solid polymer electrolyte preparation:

An electrolyte casting solution was prepared by adding ACN and PC via syringe to blue cap bottle containing $LiClO_4$. Then the PMMA was slowly added in the solution, followed by stirring at 60 °C for 12 h. The gel electrolyte is formed with a weight percent composition of 61:17:7:15 (ACN: PC: $LiClO_4$: PMMA). After assembling a device, the gel electrolyte will change to solid electrolyte after naturally dried in air for 2 h.

2.3 Sample characteristics:

The surface tension and viscosity of the ink were analyzed by Kibron Ez-Pi Plus and Brookfield viscometer, respectively. The X-ray diffraction (XRD, Bruker D8 Discover diffractometer with Ni-filtered CuKα-radiation (λ = 1.5406 Å)), transmission electron microscope (TEM, JEOL 2010), scanning electron microscopy (SEM, JEOL 7600F), optical microscope (Olympus SZ61) were used to characterize the morphology, structure and composition of the products. The adhesion strength was evaluated according to ASTM D3359, standard test methods for measuring adhesion by tape testing. X-ray photoelectron spectroscopy (XPS) analysis of the NiO and WO_3 powder was performed using the VG ESCALab 220i-XL Imaging XPS last calibrated in March 2015. Monochromatic Al K_α X-ray gun (hν =1486.7 eV) was employed using a large area lens mode for analysis with photoelectron take-off angle of 90°

with respect to surface plane. The maximum analysis depth lies in the range of 4 – 8 nm. The error of binding energy is estimated to be within ± 0.2 eV.

2.4 Electrochemical Characterization:

The electrochemical measurements of NiO films were performed on a Solartron 1470E. The transmission spectra of NiO thin films and the solid device in the fully colored and fully bleached states were measured on a SHIMADZU UV-3600 spectrophotometer over the wavelength range from 300 to 900 nm.

3. Results and discussion

3.1 Microstructure characteristics

To determine the crystal structure and phase information of the NiO and the WO_3 powder, XRD patterns were collected from both samples as shown in Fig. 1a. The XRD spectra of the synthesized NiO powder exhibits diffraction peaks at 2θ degree of 37.78°, 43.31°, 62.74°, 75.49° and 79.49°, which can be assigned to (111), (200), (220), (311) and (222) reflections of the cubic NiO phase (JCPDS 00-047-1049), respectively. The synthesized WO_3 powder shows characteristic diffraction peaks that can be readily indexed to a mixture of hexagonal and orthorhombic $WO_3 \cdot 0.33H_2O$ (JCPDS 00-035-1001 and 00-035-0270). XPS measurements were performed to analyze the binding energy and oxidation state of the NiO and WO_3 powder. Fig. 1b shows the high resolution Ni 2p XPS spectrum of the NiO powder. Ni $2p_{3/2}$ peak includes two components, one peak at 854 eV due to Ni^{2+} in Ni–O bonds and another peak at 856 eV due to Ni–OH bonds, respectively.[33, 34] The Ni–OH bonds mainly come from NiOOH or tert-butanol groups attached to the surface of NiO.[35] It illustrates that the powder present is mainly NiO, and possibly contains small amount of NiOOH on the surface of NiO nanoparticles. There are spin–

orbit doublets in the high resolution XPS spectrum of the W4f peak, corresponding to $W4f_{7/2}$, $W4f_{5/2}$ and $W5p_{3/2}$ peaks which are located at 35.7 eV, 37.8 eV and 41.5 eV, respectively (Fig. 1c). These results match well with those reported in previous literatures for WO_3.[36, 37] Fig. 1d and e present the TEM images of the NiO and WO_3 powder, respectively. The NiO nanoparticles show non-agglomerated, defined particles with a particle size distribution of 30~50 nm (Fig.1d). HRTEM image shows that lattice fringes with interplanar spacings of d_{200} =0.21nm is clearly imaged, consistent with the cubic rock salt structure of NiO deduced from XRD patterns. Fig.1e shows that the WO_3 nanoparticles are quasi-oblong in shape, and the sizes vary from 50~120 nm. The lattice fringe distances of 0.32 nm in the HRTEM image is in agreement with the the d-spacings of (200) planes of hexagonal $WO_3 \cdot 0.33H_2O$. It is worth noting that both NiO and WO_3 particle sizes are suitable for inkjet printing applications with the typical nozzle diameter in the range of tens of micrometers. The surface morphologies of the NiO and the WO_3 films printed on ITO glass are shown in SEM images of Fig. 1f and g, respectively. Uniform particles with compact smooth surface are observed in the printed NiO film (Fig. 1f). The printed WO_3 film is assembled from many smaller nanoparticles (Fig. 1g). The thickness of the printed films is proportionally increased by increasing the number of printed layers. The thickness of the printed NiO films with 1, 2 and 3 layers is 170, 335 and 530 nm as shown in Fig. S1a, b and c in Supporting Information, respectively. In addition, the thickness of the printed WO_3 films (5 wt.%) with 1 layer is 218 nm. The adhesion of the printed films on the ITO substrate was studied using the standard American Society for Testing and Materials Procedure (ASTM D3359), in which ASTM 0B and 5B represent the worst and the highest adhesion grade, respectively. Fig. S2a shows the optical microscope image of WO_3 films on ITO glass after tape test. The edges of the cuts are completely smooth and none of the squares of the lattice is detached. Therefore, the

film exhibited the highest adhesion grade of 5B. From the SEM image (Fig. S2b), it can be seen that there is no obvious change for the WO_3 film after tape test, the WO_3 nanoparticles stayed in the original positions and kept their shapes on the ITO substrate, which indicates that the printed films exhibit strong adhesion with the ITO glass.

3.2 Electrochemical performance evaluations

Electrochromic properties of the printed NiO films with different layers were measured in a three–electrode electrochemical cell containing 1 M KOH aqueous solution as the electrolyte. The printed NiO films were used as the working electrode, a Pt wire was used as the counter electrode and an Ag wire was used as the reference electrode. The transmittance of the ITO glass in the electrolyte was considered to be 100 % and was used as the baseline. The color of the NiO films changed from transparent (bleached state) to brown (colored state) when applying step voltages of -0.2 and 0.6 V (vs. Ag wire). The coloration and bleaching process of the NiO films can be attributed to the following electrochemical reactions:

$$NiO + OH^- \leftrightarrow NiOOH + e^- \quad (1)$$

The transmittance spectra of the printed NiO films with different layers at colored and bleached states in the wavelength range of 300–900 nm are shown in Fig. 2a. It is clearly seen that the transmittance of the NiO films at both colored and bleached states decreases with increasing the number of NiO layers, and the optical modulation increases linearly with increasing number of NiO layers within 3 layers (Fig. 2b). However, the optical modulation decreases dramatically for the printed NiO over 3 layers, because the films can hardly be bleached due to the thick dense layer in the presence of organic binder with larger amount NiO nanoparticles. Switching speed from one state to another state under alternating potential is an important factor in electrochromic devices. Herein, the switching time is defined as the time required for a system to reach 90% of

its full optical modulation. The coloration and bleaching times of the printed NiO films with different layers are investigated by employing chronoamperometry (CA) and the corresponding in-situ transmittance at 550 nm, as shown in Fig. 2c and Fig. S3. It can be clearly seen that both switching time generally increases with increasing number of the NiO layers, and the coloration time is shorter than bleaching time for all the films, which illustrated that the coloration process is easier than the bleaching process for all the printed NiO films. Coloration efficiency (CE) is another important criteria often used to characterize an electrochromic material, which is defined as the ratio of optical density change (ΔOD) of the film at a certain wavelength and corresponding injected (or ejected) charge density (Q) per unit area. It can be calculated according to the following equation:

$$CE(\lambda)=\frac{\Delta OD(\lambda)}{\Delta Q} \tag{2}$$

$$\Delta OD(\lambda)=\log\frac{T_b}{T_c} \tag{3}$$

where T_b and T_c denote transmittance of the film in bleached and colored states, respectively. The variation tendency of the CE (Fig. 2d) is similar with that of the optical modulation, which increases with increasing number of NiO layers within 3 layers, and then decreases over 3 NiO layers. The values of the CE are in the range from 47.3 to 66.5 $cm^2\ C^{-1}$.

Based on the above results, the optical modulation and CE of the printed NiO films are not continuously increasing with increasing number of NiO layers due to the restricted bleaching process of thick NiO films in the presence of organic binder, which can retard the diffusion of electrolyte into the thick NiO layer. The increasing number of NiO printed layers is beneficial to the electrochromic performance within 3 layers, however, the continuous increasing of NiO printed layers poses adverse effect on the electrochromic performance after 3 layers.

In order to verify this, the printed NiO films with 6 layers undergone annealing at different temperature for 2 h were further investigated. SEM images of the films after annealing at different temperature are shown in Fig. 3. The exposure of pristine NiO particles of the film annealed at 150 °C was due to the partial evaporation of organic solvent and thus the film exhibits porous structure (Fig. 3a). After annealing at 200 °C, most of the organic solvent was evaporated and uniform NiO nanoparticles were left behind as shown in Fig. 3b. However, the NiO nanoparticles begin to aggregate when the annealed temperature is up to 250 °C (Fig. 3c) and the NiO nanoparticles show strong agglomeration after annealing at 300 °C (Fig. 3d). To determine the crystal structure and possible phase changes during the annealing process, XRD patterns are collected from the films after annealing at various temperatures as shown in Fig. S4. It can be clearly seen that the diffraction peaks of the films remain unchanged. After subtracting the diffraction peaks of substrates, the diffraction peaks at 2θ degrees of 37.78°, 43.31° and 62.74° can be assigned to (111), (200) and (220) reflections of the cubic NiO phase, respectively.

Electrochromic properties of the printed NiO films with 6 layers after annealing at different temperature for 2 h were further measured in the three–electrode electrochemical cell. Fig. 4a shows the transmittance spectra of the printed NiO films with 6 layers after annealing at different temperature for 2 h at colored and bleached states in the wavelength range of 300–900 nm. It can be seen that the transmittance of the NiO films at both colored and bleached states increases with increasing the annealed temperature due to the evaporation of the organic solvent and the decomposition of the organic binder, leading to active electrochemical reaction of NiO with the electrolyte. The optical modulation increases with increasing annealed temperature within 200 °C, and then decreases when the annealed temperature is over 200 °C (Fig. 4b). A higher annealing temperature typically leads to the formation of compact crystalline NiO.[38, 39] A fully

crystalline and agglomerated film is considered too dense for ion intercalation, thus resulting in low electrochromic performance. The film almost could not color after annealing at 300 °C for 2 h due to the serious aggregation of the NiO nanoparticles that is not permeable to the ions diffusion within the bulk of NiO and lead to limited coloration reactions. Therefore, the increased optical modulation and the transmittance of the NiO films at colored states after annealing at 150 °C and 200 °C can be attributed to the evaporation of the organic binder and the porous structure of the film. However, the aggregation of the film annealed at 250 °C and 300 °C will hinder the electrochromic reaction. The coloration and bleaching times of the printed NiO films with 6 layers after annealing at different temperature for 2 h were investigated by CA and the corresponding in situ transmittance at 550 nm (Fig. 4c and Fig. S5). It can be clearly seen that bleaching time in general decreases with increasing annealing temperature, and the coloration time of the annealed films is shorter than that of the unannealed NiO film, but with slight increase with increasing annealing temperature after 200 °C. The variation of the CE is similar with that of the optical modulation as shown in Fig. 4d. The values of the CE are in the range from 25.3 to 73.7 cm^2 C^{-1}. These results further illustrate that annealing at high temperature promotes the bleaching process, but coloration process suffers a trade-off. Considering these factors, the optimal temperature for annealing of printed NiO films is 200 °C.

Electrochromic properties of the printed NiO films with different layers undergone annealing at 200 °C for 2 h were also further measured in the three–electrode electrochemical cell. It can be seen from Fig. 5a and b that though the transmittance of the NiO films at both colored and bleached states decrease with increasing the number of NiO layers, the optical modulation of the films increases linearly. This proves that the removal of organic binder helps in facilitating ion diffusion in thick layers. The largest optical modulation of the printed NiO

films is 64.2 % at 550 nm for the 9 layers. The optical modulation of 64.2% is comparable to that of the NiO film prepared by reactive dc magnetron sputtering (70%)[40], electrodeposition[41] and hot-filament metal-oxide vapor deposition[42], but much higher than that of the NiO films obtained from pulsed laser deposition (48%)[43] and oxidation in air (37%)[44].The coloration and bleaching time of the printed NiO films undergone annealing at 200 °C for 2 h, as predicted, are increasing with increasing the number of NiO layers as shown in Fig. 5c and Fig. S6, but faster than that of the corresponding unannealed NiO films. In general, the bleaching time is shorter than that of the colored time. The CE increases with increasing number of NiO layers (Fig. 5d). The CE value of the printed film with 9 NiO layers is 136.7 cm^2 C^{-1}, which is comparable to that of the NiO film prepared via electrodeposition technique (107 cm^2 C^{-1})[45], but much higher than that of the NiO films prepared by chemical bath deposition (33.9 cm^2 C^{-1})[46] and aerosol-assisted chemical vapor deposition (45 cm^2 C^{-1})[47].

To evaluate the electrochromic properties of the solid device, the printed NiO film with 3 layers as ion storage layer, WO_3 film with 3 layers as electrochromic layer, PMMA-based polymer electrolyte as the solid electrolyte were assembled with the configuration as shown in Fig. 6a. Before assembled into electrochromic devices, both printed NiO and WO_3 films were annealed at 200 °C for 2 h. The thickness of the NiO and WO_3 films is 450 and 635 nm, respectively, as shown in Fig. S7. For comparison, a solid device without NiO film was also prepared with the same WO_3 film and electrolyte, just replacing the NiO film by a piece of bare ITO glass. The transmittance spectra of the solid electrochromic devices in the colored and bleached states were measured at -2.5 and 2.5 V for 30 s, respectively. It can be seen from Fig. 6b that the solid device with NiO film as ion storage layer showed an optical modulation of 75% at 633 nm, which is much larger than that of the device using bare ITO complementary electrode

without NiO film (18.8%) and other complementary all solid-state electrochromic devices recently reported.[48-50] The digital photos of the solid device with NiO film as ion storage layer in bleached state and colored state are shown in the inset of Fig. 6b and a pattern device in colored state and bleached state are shown in Fig. 6c. The switching speed characteristics of the solid electrochromic devices were studied by employing CA and the corresponding in situ transmittance at 633 nm, as shown in Fig. S8a. The coloration and bleaching time of the solid device with NiO film as ion storage layer is 10.0 and 13.1 s, respectively, which is longer than that of the solid device without NiO film (12.5 and 5.9 s, respectively), but it is shorter than that of the complementary all solid-state electrochromic device previously reported (10.0 and 20 s, respectively).[51] In addition, the CE can be calculated from the curve slope of the ΔOD at a wavelength of 633 nm vs. the inserted charge density at colored state as shown in Fig. 6d. The CE of solid device with NiO film as ion storage layer is 131.9 cm^2 C^{-1}, which is more than 2 times larger than that of the solid device without NiO film. Fig. S8b shows the first 100 coloration–bleaching cycles, which vary as a function of time within 6000 s for the solid electrochromic devices. The solid device with NiO film as ion storage layer sustains a transmittance modulation of about 81.1 % of the corresponding initial values after 100 coloration–bleaching cycles. However, the solid device without NiO film only maintains a transmittance modulation of about 65.9% of its initial value after 100 cycles. Therefore, the results verify that solid device with NiO film as ion storage layer has more stable and reversible electrochromic performance. The enhancement of electrochromic performances is attributed to the synergistic contribution from NiO and WO_3 film, because the NiO film not only performs as ion storage layer, but also as complementary electrochromic layer in this case.

4. Conclusions

In summary, a versatile ink formulation was developed to prepare NiO and WO_3 inks simultaneously for inkjet printing application. The printed films have strong adhesion with the ITO glass. The number of printed layers and the annealed temperature could be selectively chosen to prepare electrochromic films with desired performance. The printed NiO with 9 layers undergone annealing at 200 °C for 2 h exhibits an optical modulation of 64.2% and a CE of 136.7 cm^2 C^{-1}. In addition, an all solid device was assembled with printed NiO film as ion storage layer, printed WO_3 film as electrochromic layer, PMMA-based polymer electrolyte as the solid electrolyte which shows larger optical modulation, higher CE and more stable cycling performance than that of the solid device without NiO film. The enhancement of electrochromic performance is attributed to the synergistic contribution from NiO and WO_3 film, because the NiO film not only performs as ion storage layer, but also as complementary electrochromic layer.

Acknowledgments

This research is supported by A*Star–MND Green Building Joint Grant 1321760013. Part of the work is also supported by NTU–HUJ–BGU Nanomaterials for Energy and Water Management Programme under the Campus for Research Excellence and Technological Enterprise (CREATE) and the National Research Foundation Competitive Research Programme, Award No. NRF-CRP–13–2014–02, that is supported by the National Research Foundation, Prime Minister's Office, Singapore.

References

1 A. Llordes, G. Garcia, J. Gazquez and D.J. Milliron, *Nature,* 2013, **500**, 323-326.

2 X. Xie, K. Kretschmer and G. Wang, *Nanoscale*, 2015, **7**, 13278-13292.

3 S. Vankova, S. Zanarini, J. Amici, F. Camara, R. Arletti, S. Bodoardo and N. Penazzi, *Nanoscale*, 2015, **7**, 7174-7177.

4 G.A. Niklasson and C.G. Granqvist, *J. Mater. Chem.,* 2007, **17**, 127-156.

5 H. Jiang, D.Y. Ren, H.F. Wang, Y.J. Hu, S.J. Guo, H.Y. Yuan, P.J. Hu, L. Zhang and C.Z. Li, *Adv. Mater.*, 2015, **27**, 3687-3695.

6 H. Jiang, Y.J. Hu, S.J. Guo, C.Y. Yan, P. S. Lee and C.Z. Li, *ACS Nano*, 2014, **8**, 6038-6046.

7 C.-G. Granqvist, *Nat. Mater.,* 2006, **5**, 89-90.

8 M.Q. Cui, W.S. Ng, X. Wang, P. Darmawan and P.S. Lee, *Adv. Funct. Mater.,* 2015, **25**, 401-408.

9 X.H. Yang, G. Zhu, S.H. Wang, R. Zhang, L. Lin, W.Z. Wu and Z.L. Wang, *Energy Environ. Sci.,* 2012, **5**, 9462-9466.

10 M. Gratzel, *Nature*, 2001, **409**, 575-576.

11 C.G. Granqvist, *Sol. Energy Mater. Sol. Cells,* 2000, **60**, 201-262.

12 C.Y. Yan, W.B. Kang, J.X. Wang, M.Q. Cui, X. Wang, C.Y. Foo, K.J. Chee and P.S. Lee, *ACS Nano,* 2013, **8**, 316-322.

13 X. Liu, A. Zhou, Y. Dou, T. Pan, M. Shao, J. Han and M. Wei, *Nanoscale*, 2015, **7**, 17088-17095.

14 G.F. Cai, J.P. Tu, J. Zhang, Y.J. Mai, Y. Lu, C.D. Gu and X.L. Wang, *Nanoscale,* 2012, **4**, 5724-5730.

15 F. Lin, D. Nordlund, T.-C. Weng, R.G. Moore, D.T. Gillaspie, A.C. Dillon, R.M. Richards and C. Engtrakul, *ACS Appl. Mater. Interfaces,* 2012, **5**, 301-309.

16 S.H. Baeck, K.S. Choi, T.F. Jaramillo, G.D. Stucky and E.W. McFarland, *Adv. Mater.,* 2003, **15**, 1269-1273.

17 Y. Zhou, D.H. Gu, Y.Y. Geng and F.X. Gan, *Mater. Sci. Eng. B,* 2006, **135**, 125-128.

18 A. Karuppasamy, *Appl. Surf. Sci.,* 2013, **282**, 77-83.

19 M.S. Wu and C.H. Yang, *Appl. Phys. Lett.,* 2007, **91**, 033109.

20 E. Khoo, P.S. Lee and J. Ma, *J. Eur. Ceram. Soc.,* 2010, **30**, 1139-1144.

21 F. Cao, G.X. Pan, X.H. Xia, P.S. Tang and H.F. Chen, *Electrochim. Acta,* 2013, **111**, 86-91.

22 J. Zhang, J.P. Tu, X.H. Xia, X.L. Wang and C.D. Gu, *J. Mater. Chem.,* 2011, **21**, 5492-5498.

23 J.-S. Yu, I. Kim, J.-S. Kim, J. Jo, T.T. Larsen-Olsen, R.R. Sondergaard, M. Hosel, D. Angmo, M. Jorgensen and F.C. Krebs, *Nanoscale,* 2012, **4**, 6032-6040.

24 D. Angmo, T.T. Larsen-Olsen, M. Jørgensen, R.R. Søndergaard and F.C. Krebs, *Adv. Energy Mater.,* 2013, **3**, 172-175.

25 C.-C. Huang, Z.-K. Kao and Y.-C. Liao, *ACS Appl. Mater. Interfaces,* 2013, **5**, 12954-12959.

26 S. Yuichi, F. Tomoaki and A. Masatoshi, *Jpn J. Appl. Phys.,* 2008, **47**, 7630–7634.

27 M. Layani, P. Darmawan, W.L. Foo, L. Liu, A. Kamyshny, D. Mandler, S. Magdassi and P.S. Lee, *Nanoscale,* 2014, **6**, 4572-4576.

28 C. Costa, C. Pinheiro, I. Henriques and C.A.T. Laia, *ACS Appl. Mater. Interfaces,* 2012, **4**, 5266-5275.

29 C. Costa, C. Pinheiro, I. Henriques and C.A.T. Laia, *ACS Appl. Mater. Interfaces,* 2012, **4**, 1330-1340.

30 G.H. Shim, M.G. Han, J.C. Sharp-Norton, S.E. Creager and S.H. Foulger, *J. Mater. Chem.,* 2008, **18**, 594-601.

31 P.J. Wojcik, L. Santos, L. Pereira, R. Martins and E. Fortunato, *Nanoscale,* 2015, **7**, 1696-1708.

32 G.F. Cai, X. Wang, M.Q. Cui, P. Darmawan, J.X. Wang, A.L.-S. Eh and P.S. Lee, *Nano Energy,* 2015, **12**, 258-267.

33 X. Sun, G. Wang, J.-Y. Hwang and J. Lian, *J. Mater. Chem.,* 2011, **21**, 16581-16588.

34 S.Y. Han, D.H. Lee, Y.J. Chang, S.O. Ryu, T.J. Lee and C.H. Chang, *J. Electrochem. Soc.,* 2006, **153**, C382-C386.

35 K. Fominykh, J.M. Feckl, J. Sicklinger, M. Döblinger, S. Böcklein, J. Ziegler, L. Peter, J. Rathousky, E.-W. Scheidt, T. Bein and D. Fattakhova-Rohlfing, *Adv. Funct. Mater.,* 2014, **24**, 3123-3129.

36 A. Benoit, I. Paramasivam, Y.C. Nah, P. Roy and P. Schmuki, *Electrochem. Commun.,* 2009, **11**, 728-732.

37 G.F. Cai, D. Zhou, Q.Q. Xiong, J.H. Zhang, X.L. Wang, C.D. Gu and J.P. Tu, *Sol. Energy Mater. Sol. Cells,* 2013, **117**, 231-238.

38 X.H. Xia, J.P. Tu, J. Zhang, X.L. Wang, W.K. Zhang and H. Huang, *Sol. Energy Mater. Sol. Cells,* 2008, **92**, 628-633.

39 R. Cerc Korošec, P. Bukovec, B. Pihlar and J. Padežnik Gomilšek, *Thermochim. Acta,* 2003, **402**, 57-67.

40 R.-T. Wen, G.A. Niklasson and C.G. Granqvist, *Thin Solid Films,* 2014, **565**, 128-135.

41 G.F. Cai, J.P. Tu, C.D. Gu, J.H. Zhang, J. Chen, D. Zhou, S.J. Shi and X.L. Wang, *J. Mater. Chem. A,* 2013, **1**, 4286-4292.

42 R.A. Patil, R.S. Devan, J.-H. Lin, Y.-R. Ma, P.S. Patil and Y. Liou, Sol. Energy Mater. Sol. Cells 112 (2013) 91-96.

43 I. Bouessaya, A. Rougier, P. Poizot, J. Moscovici, A. Michalowicz and J.M. Tarascon, *Electrochim. Acta,* 2005, **50**, 3737-3745.

44 G.F. Cai, C.D. Gu, J. Zhang, P.C. Liu, X.L. Wang, Y.H. You and J.P. Tu, *Electrochim. Acta,* 2013, **87**, 341-347.

45 A.C. Sonavane, A.I. Inamdar, P.S. Shinde, H.P. Deshmukh, R.S. Patil and P.S. Patil, *J. Alloys Compd.*, 2010, **489**, 667-673.

46 G.F. Cai, J.P. Tu, D. Zhou, L. Li, J.H. Zhang, X.L. Wang and C.D. Gu, *J. Phys. Chem. C*, 2014, **118**, 6690-6696.

47 M.Z. Sialvi, R.J. Mortimer, G.D. Wilcox, A.M. Teridi, T.S. Varley, K.G.U. Wijayantha and C.A. Kirk, *ACS Appl. Mater. Interfaces*, 2013, **5**, 5675-5682.

48 R. Ramadan, H. Kamal, H.M. Hashem and K. Abdel-Hady, *Sol. Energy Mater. Sol. Cells,* 2014, **127**, 147-156.

49 C.-C. Jaing, C.-J. Tang, C.-C. Chan, K.-H. Lee, C.-C. Kuo, H.-C. Chen and C.-C. Lee, *Appl. Opt.,* 2014, **53**, A154-A158.

50 K.J. Patel, M.S. Desai and C.J. Panchal, *J. Solid State Electrochem.,* 2015, **19**, 275-279.

51 J. Zhang, J.P. Tu, X.H. Xia, Y. Qiao and Y. Lu, *Sol. Energy Mater. Sol. Cells*, 2009, **93**, 1840-1845.

Figure captions

Fig. 1 a) XRD patterns of the NiO and WO_3 powder, b) Ni 2p XPS spectra of NiO powder, c) W 4f XPS spectrum of WO_3 powder, Low magnification and high magnification TEM images of the d) NiO and e) WO_3 powder, SEM images of the printed f) NiO and g) WO_3 films.

Fig. 2 a) Optical transmittance spectra at colored and bleached states, b) corresponding in transmittance modulations, c) coloration time and bleaching time and d) CE values of printed NiO films with different layers.

Fig. 3 SEM images of the printed NiO films with 6 layers undergone annealing at a) 150 °C, b) 200 °C, c) 250 °C and d) 300 °C for 2h.

Fig. 4 a) Optical transmittance spectra at colored and bleached states, b) corresponding in transmittance modulations, c) coloration time and bleaching time and d) CE values of printed NiO films with 6 layers undergone annealing at different temperature.

Fig. 5 a) Optical transmittance spectra at colored and bleached states, b) corresponding in transmittance modulations, c) coloration time and bleaching time and d) CE values of printed NiO films with different layers undergone annealing at 200 °C temperature for 2 h.

Fig. 6 a) Setup of solid electrochromic device with NiO as ion storage layer, b) Transmittance spectra of the solid electrochromic device with and without NiO as ion storage layer in the bleached (2.5 V) and colored (-2.5) states in the wave length range of 300 –900 nm (the digital photos of solid electrochromic device with NiO as ion storage layer on bleached state and colored state are presented in inset), c) A photograph of the pattern solid device with NiO as ion storage layer on bleached state and colored state, d) The

variation of the in situ optical density (ΔOD) vs. the charge density for the solid electrochromic device with and without NiO as ion storage layer.

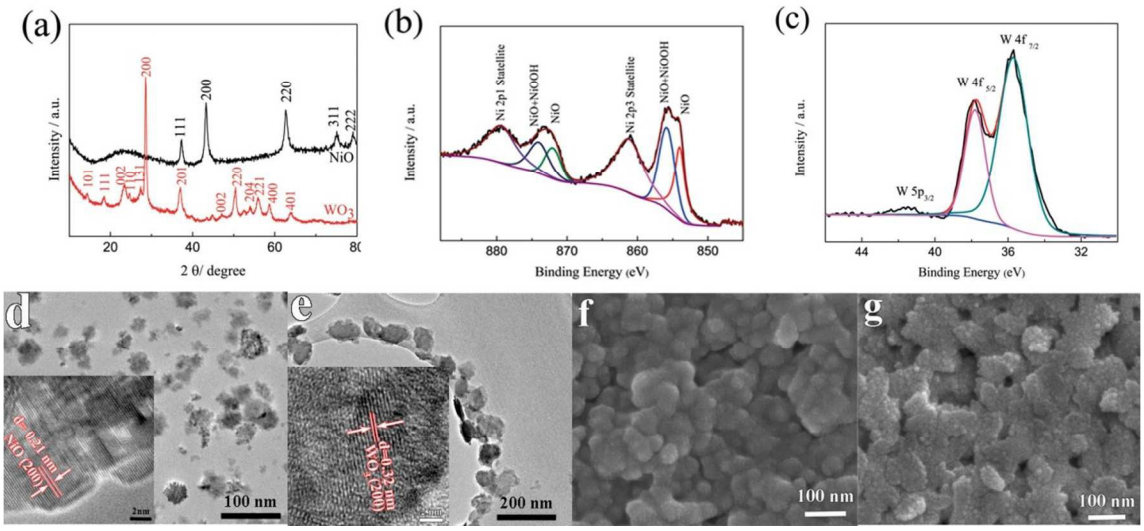

Fig.1

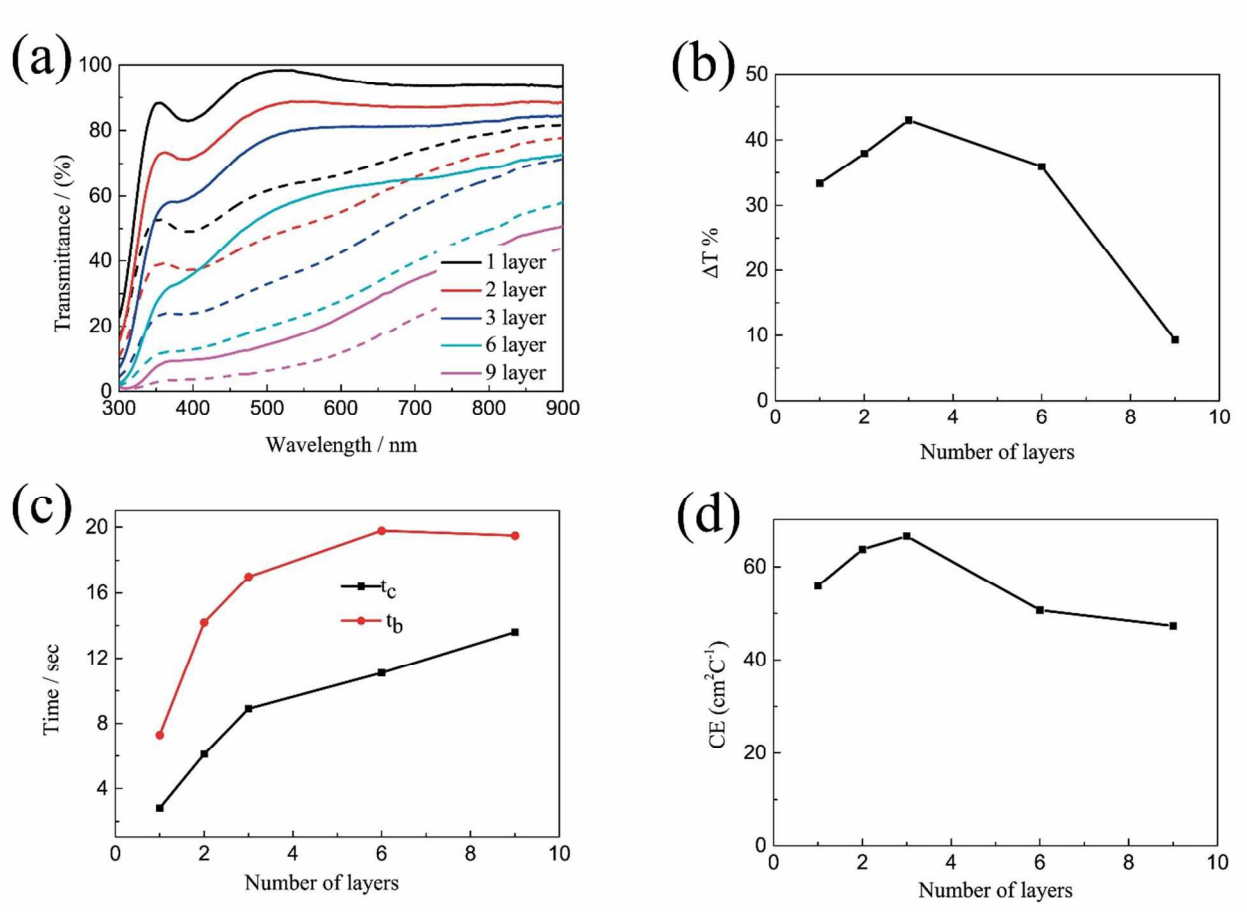

Fig. 2

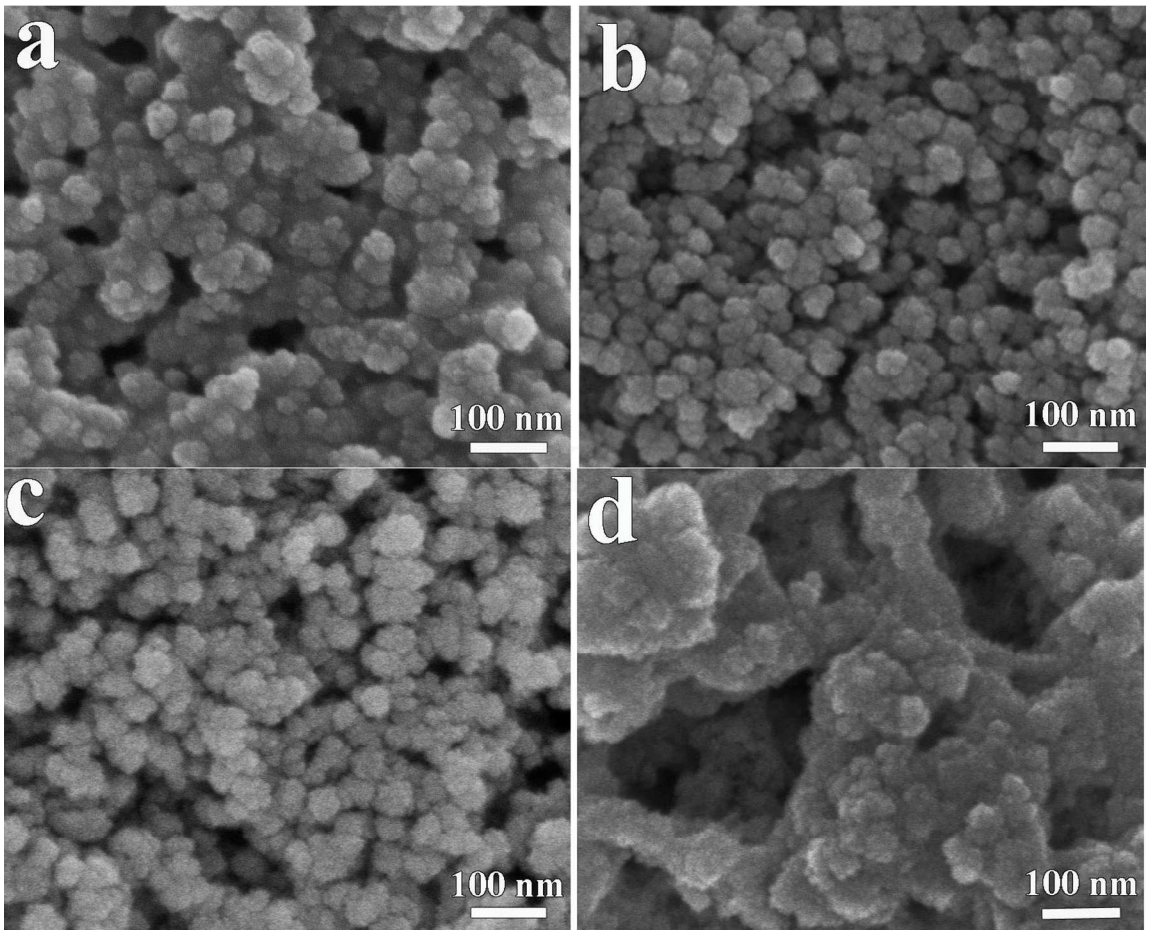

Fig. 3

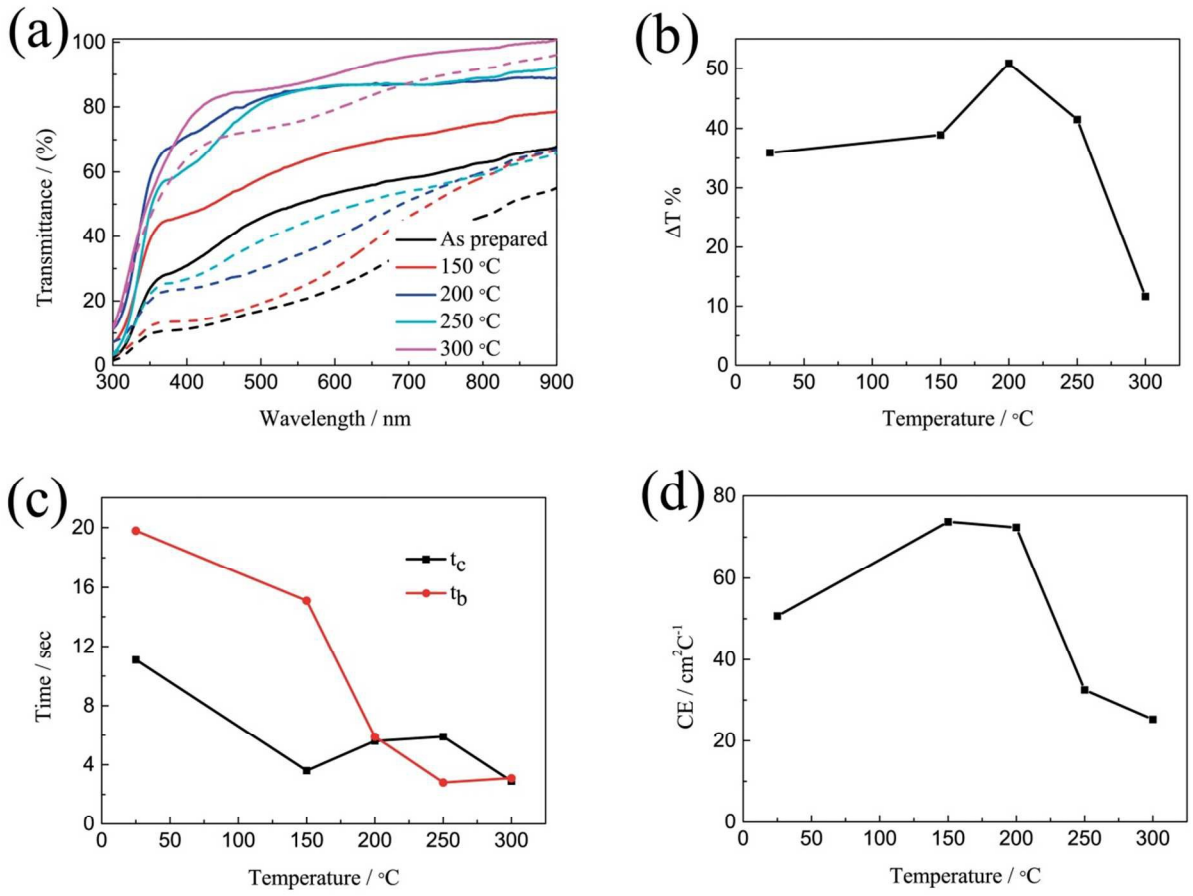

Fig. 4

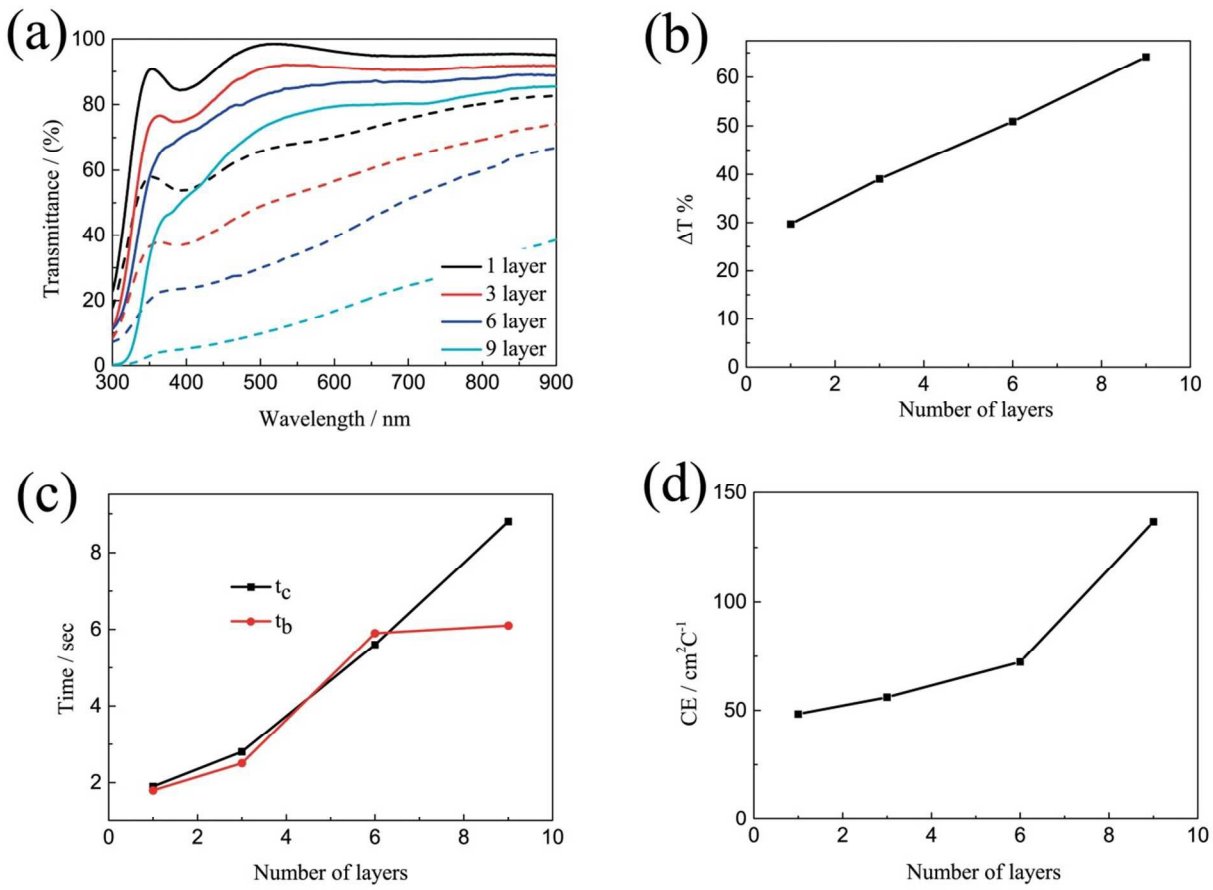

Fig. 5

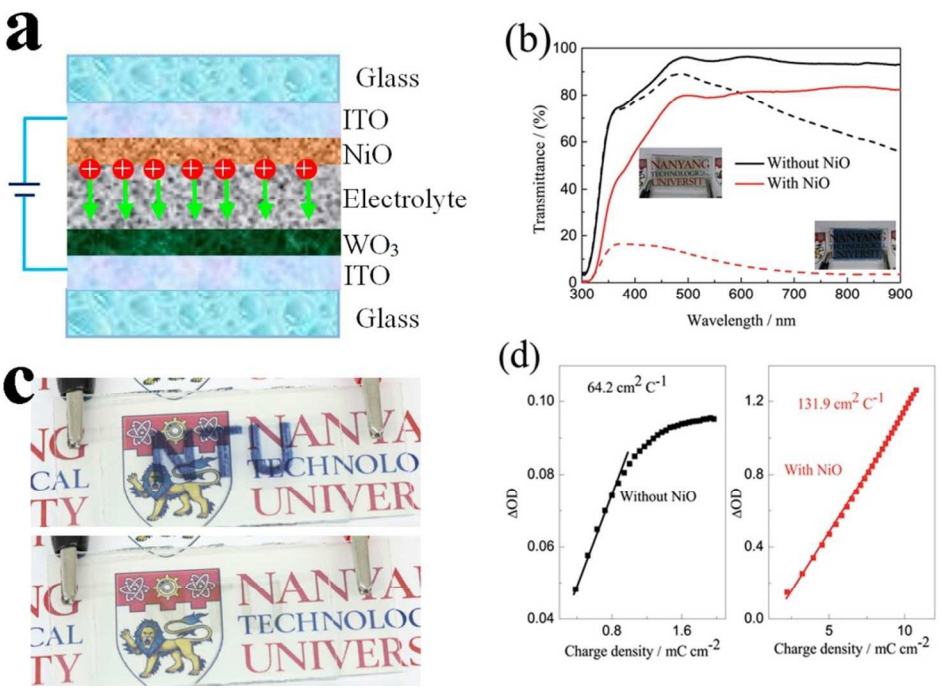

Fig. 6